NUCLEAR SCIENCE AND TECHNIQUES **26**, 030201 (2015)

Improving oxidation resistance of Ni-16Mo-7Cr-4Fe nickel-based superalloy by yttrium microalloying*

LI Xiao-Li (李晓丽),[1] HE Shang-Ming (何上明),[2,†] ZHOU Xing-Tai (周兴泰),[1]
LI Zhi-Jun (李志军),[1] ZOU Yang (邹杨),[1] LI Ai-Guo (李爱国),[2] and YU Xiao-Han (余笑寒)[1,‡]

[1] *Shanghai Institute of Applied Physics, China Academy of Sciences, 2019 Jialuo Road, Shanghai 201800, China*
[2] *Shanghai Synchrotron Radiation Facility (SSRF), Shanghai Institute of Applied Physics, Chinese Academy of Sciences, 239 Zhangheng Road, Shanghai 201204, China*

(Received July 8, 2014; accepted in revised form September 9, 2014; published online June 20, 2015)

Microstructure and oxidation behavior of modified Ni-16Mo-7Cr-4Fe alloys by yttrium microalloying were investigated by scanning electron microscopy, transmission electron microscopy, grazing incident X-ray diffraction and synchrotron radiation X-ray fluorescence. M_6C and $Ni_{17}Y_2$ phases were observed and the amount of $Ni_{17}Y_2$ increased with yttrium concentration. When the yttrium concentration increased to 0.43 wt.%, some $Ni_{17}Y_2$ chains and multi phase regions containing $Ni_{17}Y_2$, M_6C and γ phase appeared, which is harmful for the oxidation resistance. The alloy containing 0.05wt.% yttrium showed the best oxidation resistance, which derives its oxidation resistance from the adequate concentration of yttrium in the solid-solution (γ phase), the formation of the protective layer of $YCrO_3$ and chromia oxide and the strengthening effect of yttrium on oxide boundaries.

Keywords: Nickel-based superalloy, Molten salt reactor, Rare earth yttrium, Microstructure, Oxidation, X-ray fluorescence

DOI: 10.13538/j.1001-8042/nst.26.030201

I. INTRODUCTION

Developing relatively clean nuclear energy is an effective way to solve the problem of energy crisis, and structural materials for nuclear reactors are crucial to their operation safety. Ni-16Mo-7Cr-4Fe alloy manufactured by Institute of Metal Research, Chinese Academy of Sciences is a nickel-based superalloy similar to Hastelloy N alloy, which was developed in 1960s for constructing a container of molten fluoride salts at Oak Ridge National Laboratory, and is known for its good performance against corrosion, oxidation, neutron irradiation and high temperature in a molten salt reactor (MSR) [1]. In China's efforts to develop the next generation MSR, Ni-16Mo-7Cr-4Fe alloy will be used as structural material to endure the harsh environment of high temperature (1073 K or even higher) of molten fluoride salts. This alloy must be protected from the external oxidation at higher temperatures, because air oxidation can lead to a leak in the cooled tube during the service process [2, 3]. The high temperature oxidation resistance performance of Ni-16Mo-7Cr-4Fe alloy does not meet the requirement of next generation MSR. This problem is expected to be solved by rare earth microalloying modification.

Yttrium, as a rare earth element, has been applied successfully in metallurgy [4–11] and chemical and surface engineering [12–17]. Recently, yttrium has been regarded as a promising alloying element for superalloys. It improves oxidation resistance of nickel-based alloys [7], Fe-Ni-Cr ternary alloys [18], Co-based alloys [19] etc. The promotion in formation of compact layers, formation of phase transformation [6, 20], formation of less harmful phases by counteraction with other deleterious elements [7, 18, 20–22] and formation of fine dendrites [23] are thought to be beneficial effects of yttrium doping. However, to the authors' knowledge, little work focuses on effects of yttrium in matrix on oxidation resistance of Ni-based superalloys. In this paper, synchrotron radiation X-ray fluorescence (SRXRF) is used to determine distribution and content of trace yttrium in the matrix, which affect microstructure and oxidation resistance of Ni-16Mo-7Cr-4Fe alloy. This study help extend the usable critical temperature of nickel-based superalloys for molten salt energy systems.

II. MATERIALS AND METHODS

Master alloys, supplied by the Institute of Metal Research, Chinese Academy of Sciences (Shenyang, China), were melted in a vacuum induction furnace, and different amounts of yttrium were added to obtain the Ni-16Mo-7Cr-4Fe alloys (G00, G05, G12, G21 and G43). The results of ICP-AES (inductively coupled plasma atomic emission spectroscopy) analysis are given in Table 1. The ingots were hot-rolled at 1453 K to sheets of about 2 mm thickness. They were homogenized at 1450 K for 10 min and aged at 1173 K for 20 h in KSL-1400X muffle furnace, followed by water-quenching. Each specimen ($22 \times 8 \times 2\,mm^3$) for testing was cut from the sheets and was grinded, polished and cleaned.

Oxidation testing was performed at 1273 K in air using a KSL-1400X muffle furnace. An ESJ180-4 electric balance, with an accuracy of 0.1 mg, was used to measure the weight

* Supported by the program of International S&T Cooperation (No. 2014DFG60230), the National Natural Science Foundation of China (Nos. 51371189 and 51371188), Science and Technology Commission of Shanghai Municipality (No. 11JC1414900) and the Scientific Research Foundation for the Returned Overseas Chinese Scholars, State Education Ministry
† heshangming@sinap.ac.cn
‡ yuxiaohan@sinap.ac.cn

TABLE 1. Chemical compositions (in wt.%) of Ni-16Mo-7Cr-4Fe alloys with different concentrations of yttrium

Alloy	Y	Mo	Cr	Fe	Mn	Si	Al	Ti	Cu	C	Ni
G00	0.00	16.10	7.32	4.15	0.41	<0.002	0.11	<0.002	0.002	0.038	Bal
G05	0.05	16.14	7.30	4.09	0.45	<0.002	0.11	<0.002	0.002	0.034	Bal
G12	0.12	16.20	7.28	4.19	0.43	<0.002	0.12	<0.002	0.002	0.036	Bal
G21	0.21	16.09	7.21	4.12	0.48	<0.002	0.11	<0.002	0.003	0.038	Bal
G43	0.43	16.23	7.37	4.20	0.39	<0.002	0.15	<0.002	0.002	0.033	Bal

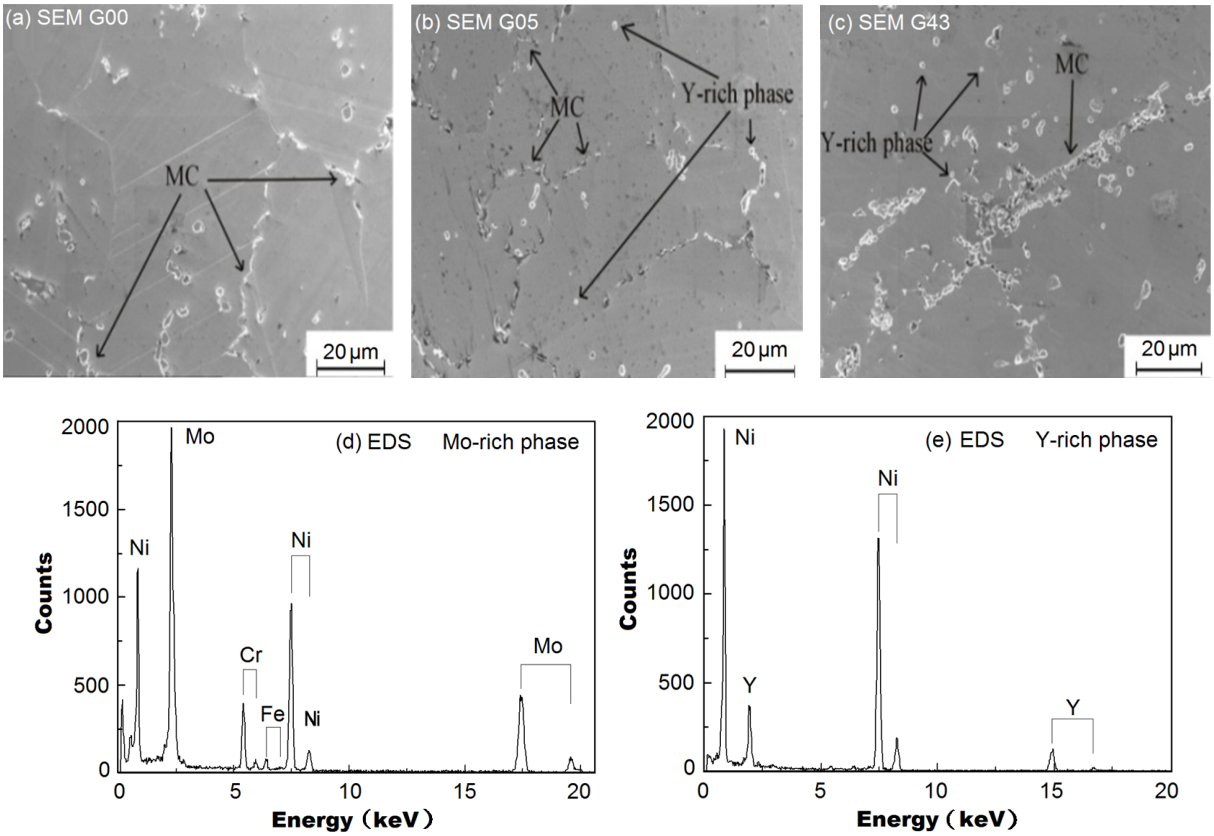

Fig. 1. SEM images of Ni-16Mo-7Cr-4Fe alloys with various yttrium concentrations.

change of each specimen (five specimens were tested to obtain an average) after completion of each exposure period. Microstructure of the specimens before and after oxidation test was observed using a LEO 1530VP scanning electron microscope (SEM) and a Tecnai G^2 F20 transmission electron microscope (TEM) with an energy dispersive spectroscopy (EDS). X-ray fluorescence (XRF) at 20.5 keV and grazing incidence X-ray diffraction (GIXRD) at 10.0 keV were conducted at Shanghai Synchrotron Radiation Facility (SSRF).

III. RESULTS AND DISCUSSION

Figure 1 shows SEM images of the Ni-16Mo-7Cr-4Fe alloys before oxidation. Coarse particles were observed along grain boundaries. The number of coarse particles in the alloy samples increased with yttrium concentration. The SEM-EDS results of the coarse particles indicate that there are Mo-rich and Y-rich phases. The amount of Y-rich phase observed in the Ni-16Mo-7Cr-4Fe alloys containing yttrium increased with yttrium concentration. The amount of Mo-rich phase in G05 was less than that in G00, but it increased with further enhancing yttrium concentration. TEM results indicate that the two phases were M_6C and $Ni_{17}Y_2$, respectively.

The selected area diffraction patterns (SADPs) of M_6C and $Ni_{17}Y_2$ are shown in Fig. 2. M_6C is angular and has a face centered cubic structure. $Ni_{17}Y_2$ has a hexagonal crystal structure with $a = 0.8320$ nm, $c = 0.8042$ nm and a space group of P63/mmc. Figure 3 shows TEM morphology of M_6C phase and $Ni_{17}Y_2$ phase. The shape of $Ni_{17}Y_2$ phase changed from round to irregular with increasing yttrium content. The $Ni_{17}Y_2$ phase was circular in G05 (Fig. 3(a)). It grew and became irregular shape (Fig. 3(b)). When the content of Y reached 0.43 wt.%, some multi-phase regions appeared, including M_6C and $Ni_{17}Y_2$ phases (Fig. 3(c)). The M_6C phase presented strip shape in G00 (Fig. 3(d)). However,

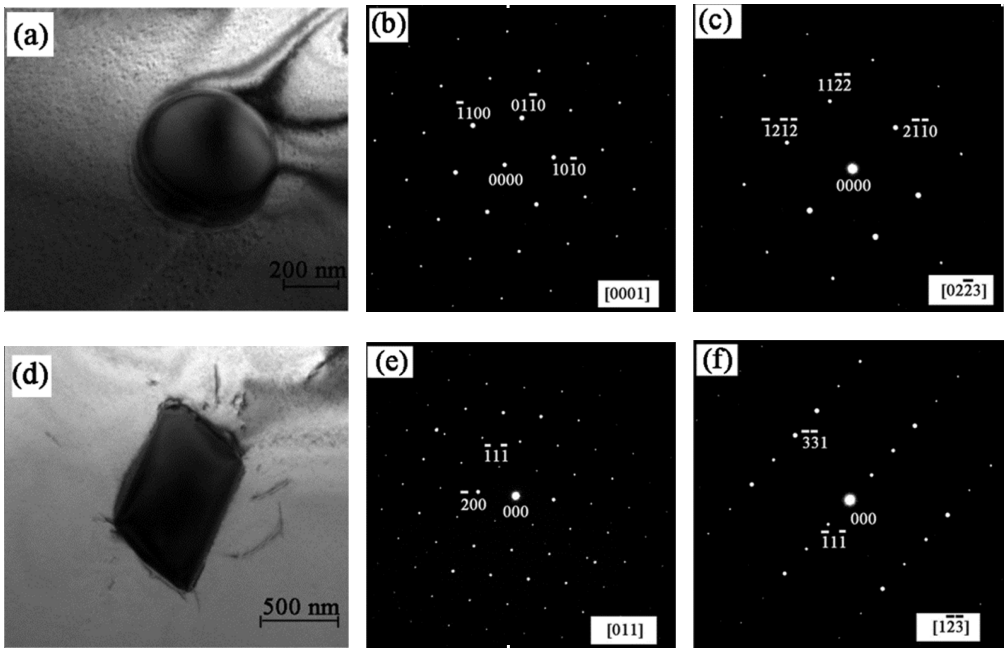

Fig. 2. TEM morphology of $Ni_{17}Y_2$ phase (a) and the SADP (b, c); and morphology of M_6C phase (d) and the SADP of M_6C (e, f).

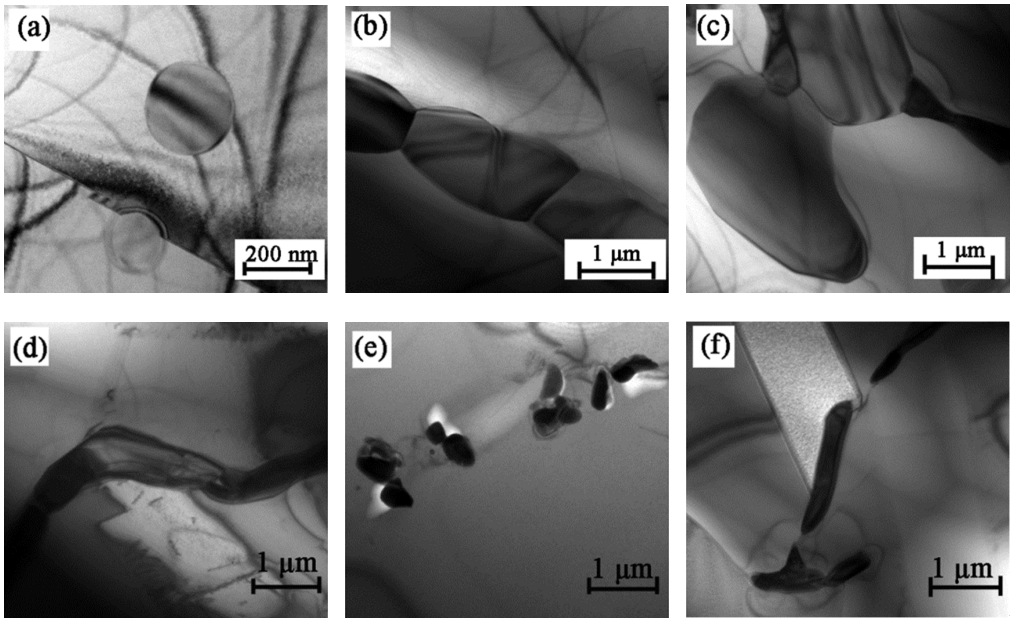

Fig. 3. TEM morphology of $Ni_{17}Y_2$ phase (a) and the SADP (b, c); and morphology of M_6C phase (d) and the SADP of M_6C (e, f).

in G05, it changed to discrete particle (Fig. 3(e)) and turned back to strip shape when further increasing yttrium concentration (Fig. 3(f)).

Oxidation curves of all specimens are shown in Fig. 4(a). It can be seen that adding yttrium into Ni-16Mo-7Cr-4Fe alloy improves substantially the oxidation resistance, especially G05. However, the oxidation resistance weakens gradually with increasing yttrium concentration. So, proper yttrium improves adhesion of the oxide scale to substrate significantly (Fig. 4(b)). Severe spallation of the oxide scale of alloy G05 did not appear in 300 h. However, alloy G00 exhibited the most severe spalling, followed by alloy G43, G21 and G12.

The GIXRD results of oxide scale of G00 and G05 (Fig. 5) show that both of the outmost layers of the oxide scales are composed of NiO (PDF 65-6920) and $NiFe_2O_4$ (PDF 47-1417). Figure 6 shows the cross-sectional XRF-mapping of alloys. Unfortunately, most of the outer oxide layer of G00 and G43 spalled, and the XRF mapping area

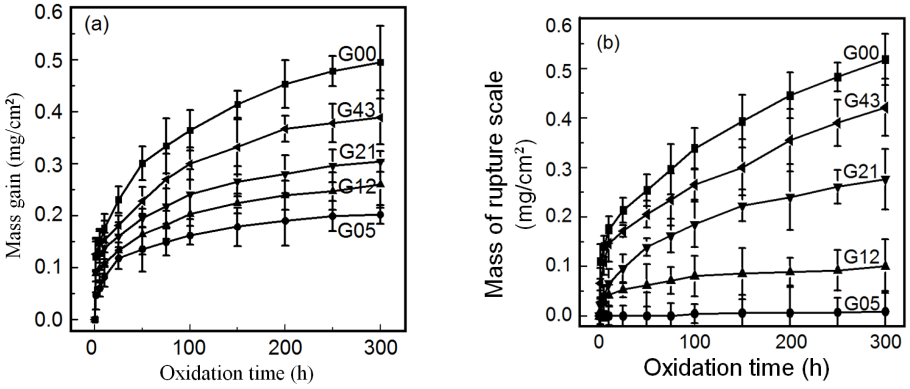

Fig. 4. Weight gain (a) and mass of rupture scale (b) as function of exposure time of the alloy specimens air-exposed at 1273 K for 300 h.

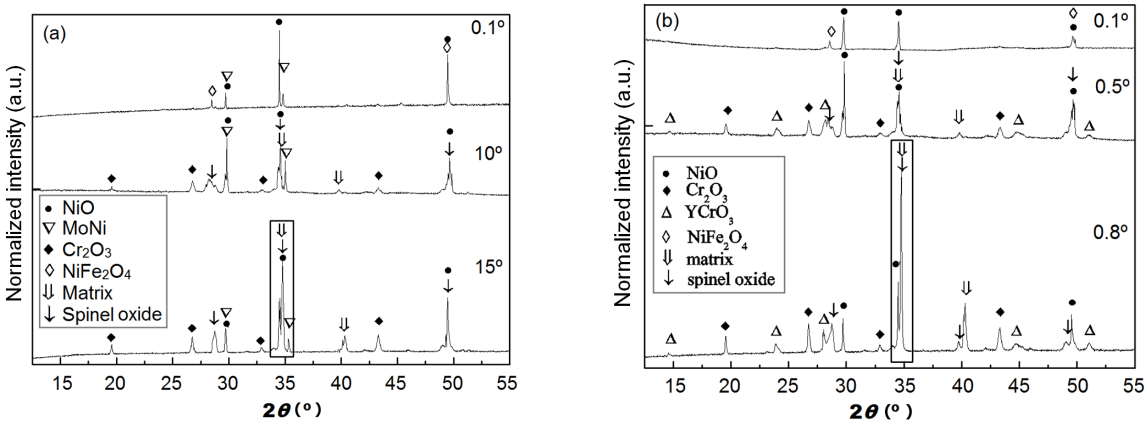

Fig. 5. Grazing incidence X-ray diffraction profiles of the oxide scales formed on specimens oxidized at 1273 K for 300 h (a) G00; (b) G05.

(100 μm × 300 μm) was so small that the outmost Ni/Fe-rich layer was not detected clearly (Fig. 6(b)). Also, the oxide scale of G05 was much thinner and more compact than that of G00 and G43 (Fig. 6). For the oxide scale on the surface of G00, there were only NiO and $NiFe_2O_4$ and MoNi (PDF 50-1270) until the incidence angle increased to about 10° (Fig. 5(a)). Cr_2O_3 (PDF 38-1479), few spinel oxides ($NiCrMnO_4$, PDF 020-0780; $NiCr_2O_4$, PDF 23-1272; $FeCr_2O_4$, PDF 24-0511) and matrix also appeared when the incidence angle increased to 10°. Moreover, diffraction peaks of NiO and $NiFe_2O_4$ remained at this higher incidence angle. When the incidence angle increased to 15°, the intensity of diffraction peak of the matrix and the spinel oxides evidently increased. However, for the surface oxide scale on alloy G05, diffraction peaks mainly corresponded to NiO and $NiFe_2O_4$ when the incidence angle was 0.1°. When the incidence angle increased to 0.5°, Cr_2O_3, $YCrO_3$, spinel oxides ($NiCrMnO_4$; $NiCr_2O_4$; $FeCr_2O_4$) and matrix also appeared. When the incidence angle increased to 0.8°, the intensity of diffraction peak of the matrix and the spinel oxides evidently increased. It can be conclude that the oxide scale of G00 is much thicker than that of G05.

The possible reasons may include the followings. One is the higher yttrium concentration in the G05 matrix G05 than in G43, which can be seen by the Y mapping in Fig. 6 and the EPMA analysis in Fig. 7. With increasing yttrium contents, the volume fraction of $Ni_{17}Y_2$ increases (Fig. 7(a)) and the yttrium concentration in the matrix decreases (Fig. 7(b)). Consequently the internal compact $YCrO_3$, Cr_2O_3 and spinel oxide layer are easier to be formed in alloy G05, hence the hindering of Mo diffusion; Another possible reason is the interfaces between coarse $Ni_{17}Y_2$ and matrix, locating in the surface of the alloys containing excess yttrium. This may supply the diffusion channels for oxygen and the oxidizable elements especially Mo. Therefore, Mo-rich layer was not observed in the oxide scale of G05 which had the smallest amount of $Ni_{17}Y_2$, while the Mo-rich layer of G00 and G43 was quite thick. Thirdly, proper yttrium can enhance the strength of grain boundaries of oxides at the surface. Figure 8 shows the morphology of surface oxide scale on Ni-16Mo-7Cr-4Fe alloys after oxidation for 100 h at 1273 K. There is no crack on the surface of G05, but some intergranular cracks appeared on the surface of G00. It was suggested that proper yttrium addition might form internal oxide boundaries where vacancies could condense and thus diminish void formation [24], hence the enhanced strength of grain boundaries of oxides.

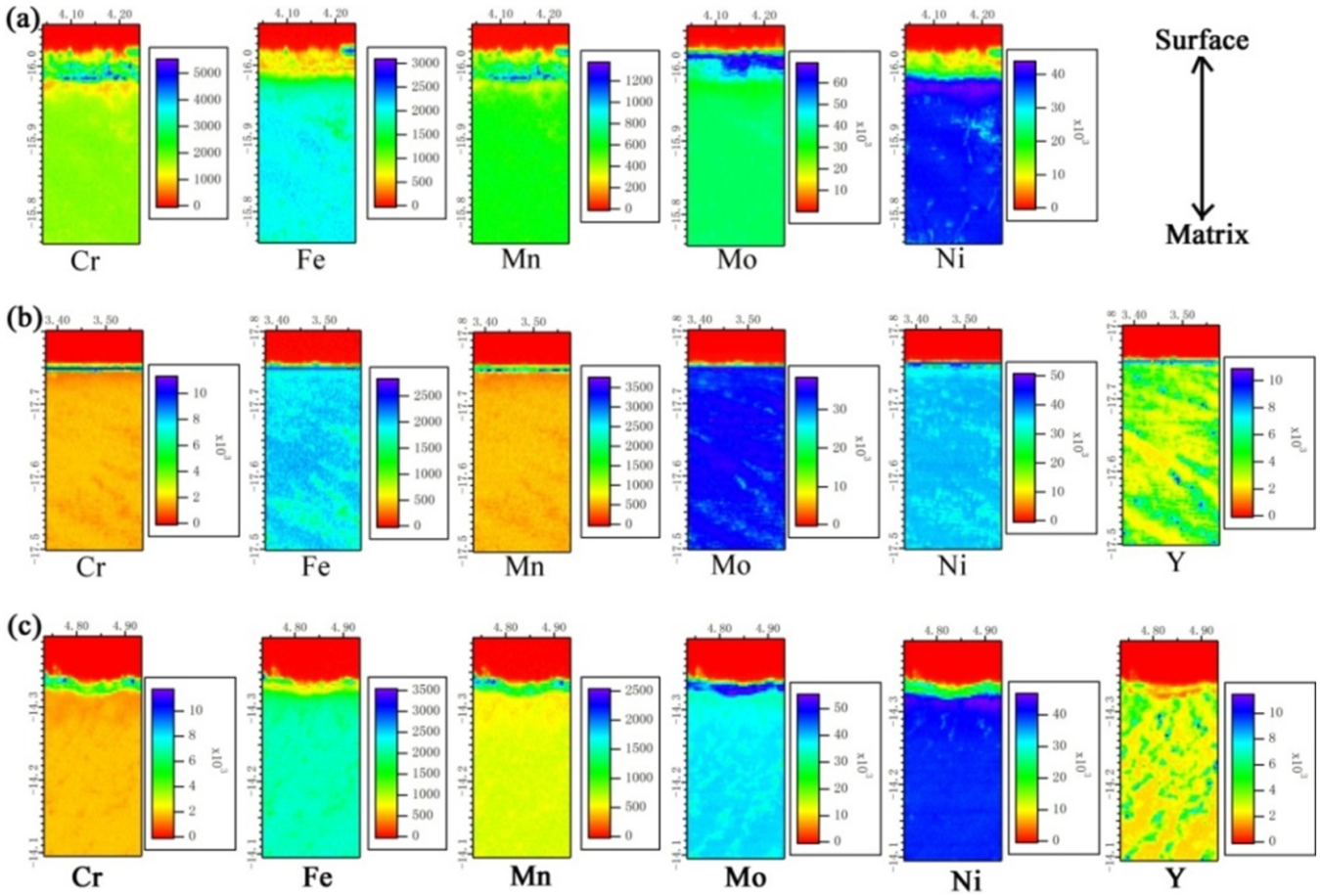

Fig. 6. (Color online) Cross-sectional XRF-mapping of the oxide scales for the specimens oxidized at 1273 K for 350 h (a) G00, (b) G05 and (c) G43.

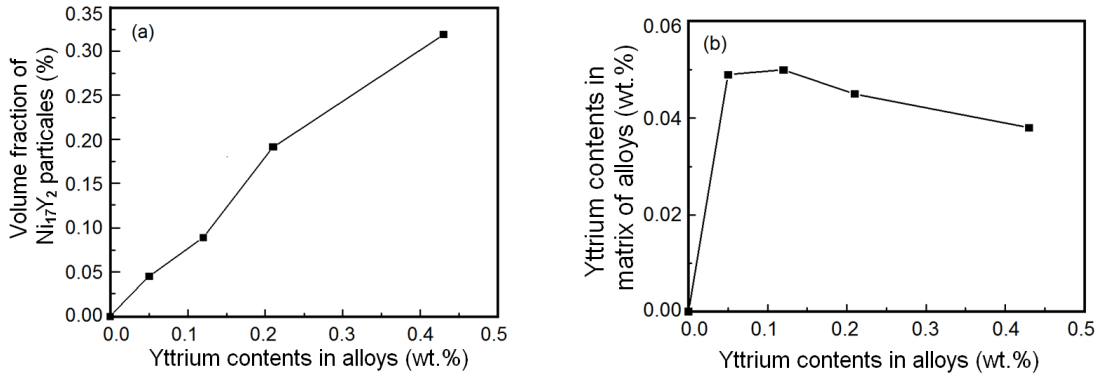

Fig. 7. EPMA analysis of the yttrium in Ni-16Mo-7Cr-4Fe alloys: (a) volume fraction of $Ni_{17}Y_2$ phase in the alloys, (b) Y contents in the matrix.

IV. CONCLUSION

Proper yttrium improves distribution of the coarse M_6C particles. The number and size of detrimental $Ni_{17}Y_2$ increase with yttrium concentration and the shape of $Ni_{17}Y_2$ changes from round to irregular. When the concentration of yttrium increases to 0.43wt.%, some coarse $Ni_{17}Y_2$ chains and multi phase regions containing $Ni_{17}Y_2$, M_6C and γ phase appear.

The oxidation resistance of Ni-16Mo-7Cr-4Fe alloy at 1273 K is improved by proper yttrium addition. The oxide scale of alloy containing 0.05 wt% yttrium is the thinnest and most compact. Proper yttrium can promote the formation of the compact $YCrO_3$ and Cr-O internal oxide layer, and then

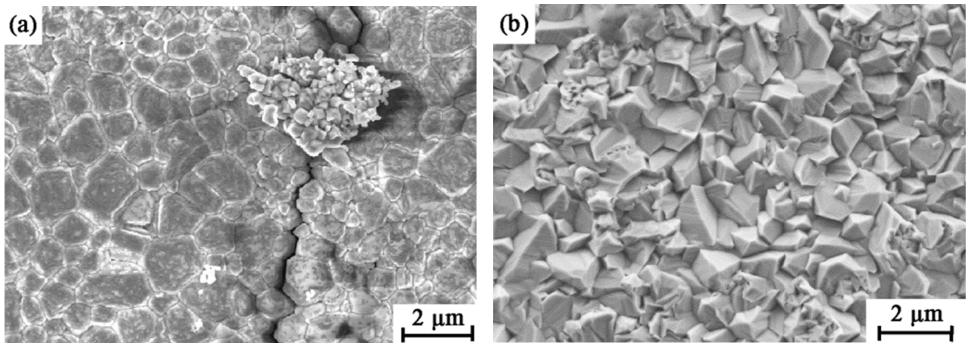

Fig. 8. Morphology of surface oxide scale on Ni-16Mo-7Cr-4Fe alloys of G00 (a) and G05 (b) after oxidation for 100 h at 1273 K.

inhibit the diffusion of Mo. With increasing yttrium concentration, the oxidation resistance of Ni-16Mo-7Cr-4Fe alloy decreases because coarse $Ni_{17}Y_2$ consumes most of yttrium in the matrix and reduces the strengthening effect of yttrium.

ACKNOWLEDGEMENTS

The authors thank staffs at the BL15U and BL14B beamline stations of SSRF.

[1] Huntley W R and Gnadt P A. Design and operation of a forced-circulation corrosion test facility (MSR-FCL-1) employing hastelloy N alloy and sodium fluoroborate salt. Oak Ridge National Laboratory Report, ORNL-TM-3863, 1973.
[2] McNeese L E. Molten salt reactor program. Oak Ridge National Laboratory Report, ORNL-5047, 1975, 125–150.
[3] McNeese L E. Molten salt reactor program. Oak Ridge National Laboratory Report, ORNL-5132, 1976, 1–15.
[4] Bullock E, Lea C, McLean M. Benefits of minor additions of yttrium to the oxidation and creep bahavior of a nickel-based composite. Philos T R Soc A, 1980, **295**: 332–333. DOI: 10.1098/rsta.1980.0126
[5] Hsu C G and Pan J M. Reaction of yttrium with *p*-nitrochlorophosphonazo and the spectrophotometric determination of yttrium in nickel-base alloys in the presence of cerium sub-group rare earths. Analyst, 1985, **110**: 1245–1248. DOI: 10.1039/an9851001245
[6] Sato A, Sato A, Harada H, *et al*. Creep strength of yttrium doped 4th generation Ni-base single crystal superalloy. J Japan Inst Metals, 2006, **70**: 380–383. DOI: 10.2320/jinstmet.70.380
[7] Stott F H, Wood G C, Fountain J G. The influence of yttrium additions on the oxidation resistance of a directionalloy solidified Ni-Al-Cr_3C_2 eutectic alloy. Oxid Met, 1980, **14**: 135–146. DOI: 10.1007/bf00603990
[8] Vozzella P A and Condit D A. Determination of yttrium in complex nickel-base alloys using microwave dissolution and inductively coupled poupled plasma optical emission spectrometry. Anal Chem, 1988, **60**: 2497–2500. DOI: 10.1021/ac00173a013
[9] Xiao C B and Han Y F. Effect of yttrium on diffusion layer of Ni-Al-Mo-B alloy IC6 during high temperature oxidation process. Scripta Mater, 1999, **41**: 1217–1221. DOI: 10.1016/s1359-6462(99)00277-8
[10] Zhou P J, Yu J J, Sun X F, *et al*. Influence of Y on stress rupture property of a Ni-based superalloy. Mat Sci Eng A-Struct, 2012, **551**: 236–240. DOI: 10.1016/j.msea.2012.04.117
[11] Zhou P J, Yu J J, Sun X F, *et al*. Role of yttrium in the microstructure and mechanical properties of a boron-modified nickel-based superalloy. Scripta Mater, 2007, **57**: 643–646. DOI: 10.1016/j.scriptamat.2007.06.003
[12] Wang S X, Li C, Xiong B J, *et al*. Surface modification of hard alloy by Y ion implantation under different atmosphere. Appl Surf Sci, 2011, **257**: 5826–5830. DOI: 10.1016/j.apsusc.2011.01.113
[13] Ding R G, Ojo O A, Chaturvedi M C. Laser beam weld-metal microstructure in a yttrium modified directionally solidified Ni_3Al-base alloy. Intermetallics, 2007, **15**: 1504–1510. DOI: 10.1016/j.intermet.2007.05.008
[14] Lu J T, Zhu S L, Wang F H. Cyclic oxidation and hot corrosion behavior of Y/Cr-modified aluminide coatings prepared by a hybrid slurry/pack cementation process. Oxid Met, 2011, **76**: 67–82. DOI: 10.1007/s11085-010-9228-0
[15] Monceau D, Oquab D, Estournes C, *et al*. Pt-modified Ni aluminides, MCrAlY-base multilayer coatings and TBC systems fabricated by Spark Plasma Sintering for the protection of Ni-base superalloys. Surf Coat Tech, 2009, **204**: 771–778. DOI: 10.1016/j.surfcoat.2009.09.054
[16] Vilar R, Santos E C, Ferreira P N, *et al*. Structure of NiCrAlY coatings deposited on single-crystal alloy turbine blade material by laser cladding. Acta Mater, 2009, **57**: 5292–5302. DOI: 10.1016/j.actamat.2009.06.049
[17] Wang K L, Zhang Q B, Sun M L, *et al*. Rare earth elements modification of laser-clad nickel-based alloy coatings. Appl Surf Sci, 2001, **174**: 191–200. DOI: 10.1016/s0169-4332(01)00017-4
[18] Moulin P, Huntz A M, Lacombe P. Relation between selective oxidation and diffusional phenomena in Fe-Ni-Cr ternary alloys-effect of yttrium additions. Acta Metall Mater, 1980, **28**: 1295–1300. DOI: 10.1016/0001-6160(80)90085-1
[19] Zhang Y D, Zhang C, Lan H, *et al*. Improvement of the oxidation resistance of Tribaloy T-800 alloy by the additions of yttrium and aluminium. Corros Sci, 2011, **53**: 1035–1043. DOI: 10.1016/j.corsci.2010.11.038
[20] Khanna A S, Wasserfuhr C, Quadakkers W J, *et al*. Addition of yttrium, cerium and hafnium to combat the deleterious effect of sulfur impurity during oxidation of an Ni-Cr-Al alloy. Mat Sci

Eng A-Struct, 1989, **120-121**: 185–191. DOI: 10.1016/0921-5093(89)90738-7

[21] Mendis B G, Livi K J T, Hemker K J. Observations of reactive element gettering of sulfur in thermally grown oxide pegs. Scripta Mater, 2006, **55**: 589–592. DOI: 10.1016/j.scriptamat.2006.06.017

[22] Schumann E, Yang J C, Graham M J. Direct observation of the interaction of yttrium and sulfur in oxidized NiA. Scripta Mater, 1996, **34**: 1365–1370. DOI: 10.1016/1359-6462(95)00662-1

[23] Xiao C B and Han Y F. Effect of silicon on microstructure and stress rupture properties at 1100 °C of yttrium modified Ni-Al-Mo-B alloy IC6. J Mater Sci, 2001, **36**: 1027–1030. DOI: 10.1023/a:1004848528582

[24] Stringer J. Stress generation and relief in growing oxide films. Corros Sci, 1970, **10**: 513–543. DOI: 10.1016/S0010-938X(70)80036-1